Electron-impact excitation of the $(2p^2)\ ^1D$ and $(2s2p)\ ^1P^o$ autoionizing states of helium

Omer Sise and Mevlut Dogan*
Department of Physics, Afyon Kocatepe University, 03200 Afyon, Turkey

Ibrahim Okur
Department of Physics, Sakarya University, Adapazari, Turkey

Albert Crowe
School of Chemistry, Newcastle University, Newcastle, United Kingdom

(Received 9 March 2011; revised manuscript received 13 May 2011; published 5 August 2011)

An experimental study of the excitation of the $(2p^2)\ ^1D$ and $(2s2p)\ ^1P^o$ autoionizing states of helium by 250-eV electron impact is presented. The ejected-electron angular distributions and energy spectra are measured in coincidence with the corresponding scattered electrons for a scattering angle of -13° and for a range of ejected-electron angles in both the forward and backward directions. Resonance profiles are analyzed in terms of the Shore-Balashov parametrization to obtain the resonance asymmetry A_μ and yield B_μ parameters and the direct ionization cross section f. The spectra and their parameters are compared to the previous measurements of Lower and Weigold [J. Phys. B **23**, 2819 (1990)] and McDonald and Crowe [J. Phys. B **26**, 2887 (1993)]. Comparison is also made with the recent theoretical triply differential cross-section calculations based on the first and second Born approximations. In general, good qualitative agreement is found between the experimental results. Some differences are found at the forward and backward directions. These differences in the shape and magnitude of the cross sections are attributed to the different incoming electron energies used in the experiments. The second Born approximation with inclusion of the three-body Coulomb interaction in the final state agrees reasonably well with experiments in the binary region. However, the $^1P^o$ resonance yield parameter B_μ is significantly overestimated at the recoil region, giving a relatively large recoil peak, in contradiction to the experiment. There is also a discrepancy between the two theories available for the ^1D resonance yield parameter B_μ in this region. Remaining discrepancies between theories and experiments are also discussed.

DOI: 10.1103/PhysRevA.84.022705 PACS number(s): 34.80.Dp, 32.80.Zb

I. INTRODUCTION

The process of excitation with autoionization in atomic collisions is a highly correlated process involving the excitation of the target to an intermediate doubly excited resonance state which autoionizes with the emission of an electron. Helium is the simplest many-electron system for the excitation with autoionization process and has played a pivotal role in our understanding of correlated electron dynamics [1]. Since the pioneering synchrotron experiment of Madden and Codling [2] and the corresponding theoretical investigations of Fano and co-workers [3–5], the autoionizing doubly excited states have been continuously studied by several experimental and theoretical groups. With the improving performance of synchrotron radiation sources, more sophisticated photoionization experiments were performed to observe high-lying doubly excited states [6–10]. Unlike the optical method, it is possible to observe both the optically allowed and forbidden transitions by charged particle-impact experiments using electron or ion projectiles [11]. Furthermore, the autoionizing resonance profile observed by the charged particle-impact experiment depends on the momentum transfer of the projectile. The doubly excited states of helium can also be populated by the double-electron-capture process in the $^3He^{2+} + He(1s^2)$ collisions [12] or dielectronic recombination of He^+ ions [13].

The doubly excited states of helium lie above the first ionization threshold, which are strongly coupled with the He^+ continuum. These states are degenerate in energy with continuum states from the direct ionization process, resulting in their nonradiative decay, autoionization. Since the same final states can be reached by either processes, interference consequently occurs, dependent on both the magnitudes and relative phases of the competing direct and resonant amplitudes. This state-continuum interference results in the observed broad asymmetric profiles, or Fano profiles [4], in the vicinity of the doubly excited states, which is, in general, constructive on one side of the energy of the resonance state and destructive on the other.

The resonance effects due to the electron-impact excitation and decay of autoionizing states are usually investigated by either energy-loss spectroscopy of scattered electrons [14–19] or ejected-electron spectroscopy [20–28]. In general, energy spectra of electrons ejected from autoionizing states depend critically on the incident energy as well as the ejection angle. At small scattering angles and high energies dipole-allowed transitions are favored, whereas for large scattering angles and lower incident energies, optically forbidden transitions become more probable.

The dynamics of excitation with autoionization process can be uniquely determined by $(e,2e)$ experiments in which both the scattered (s) and ejected (e) electrons resulting from the same ionization event are detected simultaneously in coincidence. In such an experiment the triply differential cross section (TDCS) $d^3\sigma/dE_e\,d\Omega_e\,d\Omega_s$, i.e., a cross-section

*mdogan@aku.edu.tr

 ©2011 American Physical Society

differential in the angles of emission of the two final electrons and in one kinetic energy, is measured. The kinetic energy of the other electron is determined by energy conservation. In the asymmetric coplanar arrangement, all electrons are observed in the detection plane defined by the incident and scattered momentum vectors k_0 and k_s, respectively. In this kinematic scheme, the angular distributions of the ejected electrons at fixed scattering angle have two lobes in directions near to the momentum transfer direction θ_K, i.e., the "binary" lobe with direction θ_K and the "recoil" lobe with direction $180^\circ + \theta_K$, where $\boldsymbol{K} \equiv \boldsymbol{k}_0 - \boldsymbol{k}_s$ is the momentum transferred from the incident electron to the atom (see, for example, Refs. [29–31]). Balashov *et al.* [32] first proposed extending the idea to include autoionization. Since the distribution of ejected electrons from an autoionizing state should be symmetric about the momentum transfer inversion axis in the first Born approximation, the backward direction (recoil lobe) would be suitable to enhance the autoionizing resonances against the direct ionization background. By detecting only one of the final electrons, one can determine the doubly differential cross section (DDCS), $d^2\sigma/dE_e\,d\Omega_e$. This is equivalent to integrating the TDCS over the momenta of the undetected electrons. Both DDCS and TDCS measurements in the autoionizing region can provide very sensitive information on details of the excitation process of the resonance. Moreover, measuring triply differential $(e,2e)$ cross sections for individual resonance levels yields valuable information about electron correlations at different energy regimes as well as information about the interference in the decay channel with direct ionization.

Although $(e,2e)$ measurements provide more detailed information concerning the dynamics of the collision, the experimental investigations of the autoionization of helium by this technique are very limited. This can be attributed to the low cross sections for the process, difficulties in achieving the required energy resolution, and the complications arising from interference between the autoionizing and direct ionization processes. So far, to the best of our knowledge, only the doubly excited states below the $He^+(n = 2)$ and $He^+(n = 3)$ limits have been measured by electron impact since the cross sections decrease rapidly with increasing n. The four lowest $(2\ell 2\ell')\ ^{1,3}L$ levels, $(2s^2)\ ^1S$, $(2s2p)\ ^3P$, $(2p^2)\ ^1D$, and $(2s2p)\ ^1P^o$, have been extensively studied, due to the strong presence of the resonances in the excitation spectrum. There have been a number of such $(e,2e)$ studies on these resonances [33–44]. The first comprehensive $(e,2e)$ study was carried out by Lower and Weigold [36] for a range of incident electron energies, 100–400 eV, and scattering angles 3°, 13°, and 16°. Data for the same resonances, but with lower incident energies (<100 eV) and larger scattering angles (20°–30°), were obtained in a series of papers by the same (Flinders) group [39–41]. The Newcastle group also reported high-resolution data for the ^1S state [37] and the ^1D and $^1P^o$ states [38] at 200-eV incident energy and a 12° scattering angle. At this kinematics, the resonance profiles, in general, acquire a complicated asymmetric structure in the ejection angle range $\theta_K - 20^\circ < \theta_e < \theta_K + 20^\circ$, while they have symmetric structures in the region of the recoil peak [45,46]. The experiments of the Flinders and Newcastle groups are in coplanar asymmetric geometry. The angles of the scattered and ejected electrons are fixed and the TDCS for ionization of helium to the He^+ ground state is measured as a function of the energy of the ejected electron. Both groups have analyzed their coincidence ejected-electron spectra in terms of the so-called Shore-Balashov (or, equivalently, Fano) parametrization [32,47,48] to obtain the direct $(e,2e)$ cross section f and the resonance parameters A_μ and B_μ for the resonance states as a function of ejected-electron momentum. These parameters describe the asymmetry and the magnitude of the autoionizing contribution to the $(e,2e)$ cross sections. The results from these groups were in substantial agreement, as reviewed by Crowe *et al.* [49], showing a strong dependence on the momenta of both the ejected and scattered electrons and indicating strong interference between the direct and resonance amplitudes.

On the theoretical side, considerable progress has been made in the past two decades in the description of the resonance parameters A_μ and B_μ characterizing the ^1S, ^3P, ^1D, and $^1P^o$ autoionizing states under these kinematic conditions. The calculations show high sensitivity of the cross sections to the approximation used, especially at low and intermediate incident electron energies [50,51]. Pochat *et al.* [34] have performed calculations of the Shore-Balashov parameters in a first-order distorted-wave model, including exchange between the incident or scattered electron and the target electrons. They presented both theoretical and experimental results (without the sign of the parameters) at 100-eV incident energy and a 15° scattering angle for the ^1S, ^3P, ^1D, and $^1P^o$ autoionizing states. The results of their calculations agreed relatively well with their measurements, however, their results are not in agreement with the data of Lower and Weigold [36] at almost identical kinematics. The calculation of Tweed and Langlois [52] at 70- and 80-eV incident energies are similar to those of Pochat *et al.* [34]. Kheifets [53] has also used the distorted-wave (first) Born approximation, with exchange, to calculate the Shore-Balashov parameters and the direct $(e,2e)$ cross section for the same kinematical conditions as the equivalent data of Lower and Weigold [36]. He also introduced a Gamov factor into the direct ionization amplitude in order to take into account postcollision interaction (PCI) between the scattered and the ejected electrons in the direct ionization process. Good agreement was obtained with the 400-eV data of Lower and Weigold [36], but there was less accord with these data for the 200- and 100-eV kinematical cases. McCarthy and Shang [54] have used an equivalent local form of the distorted-wave impulse approximation for the direct ionization process and a six-state momentum space close-coupling approximation for the resonant scattering amplitudes for comparison with some of the data of Lower and Weigold [36] at 100- and 400-eV incident energies. Their results were not given in the forms of Shore-Balashov parameters, but comparison was made directly with the measured coincidence spectrum. Fair quantitative agreement was achieved with the measurements.

More sophisticated calculations have been conducted by Marchalant *et al.* [55] and Fang and Bartschat [56,57]. They have used both the first and second Born approximations to evaluate $(e,2e)$ cross sections for the ^1S, ^1D, and $^1P^o$ autoionizing states. Their calculations were compared with some of the data of Lower and Weigold [36] and McDonald and Crowe [37,38]. They showed that first-order theoretical models failed to reproduce the measured coincidence spectra. The

principal sources of disagreement between first-order theory and TDCS experiments have been in the shift of the forward and backward peaks away from the momentum transfer axis, which first-order theory does not predict, and in the magnitude of the recoil peak. Only second-order models appear to be capable of giving a correct description of the autoionization process. While the second-order calculation agrees in shape, but not in magnitude, with the experimental data for 200 and 400 eV, it is in complete disagreement with the data when the incident energy is reduced to 100 eV. At this kinematics, the ejected and scattered electrons acquire comparable energies (∼35 eV) and their PCI becomes strong. It may not be accounted for fully by second-order theory [58].

Second-order calculations with inclusion of Coulomb interactions in the final state (CIFS) for excitation of the ^1D and $^1P^o$ autoionizing states of helium by 200-eV electron impact have been reported by Godunov *et al.* [59]. They calculated the full range Shore-Balashov parameters and found a good qualitative agreement with the experimental data in the forward direction when both CIFS and second-order effects have been taken into account. However, in the direction of the recoil peak, the theoretical results of the resonance yield parameter B_μ for the $^1P^o$ state are higher than the experimental results. Recently, deHarak *et al.* [60,61] reported the noncoplanar $(e,2e)$ spectral measurements for the ^1S, ^1D, and $^1P^o$ autoionizing states for kinematics of 488-eV incident energy and a 20.5° scattering angle. They showed that the second-order distorted-wave theory in the projectile-target interaction gives good results for the resonance states. However, neither first- nor second-order calculations were able to describe the full range of their experimental results. We feel that this unsatisfactory situation for excitation with autoionization process calls for further investigation.

In this paper, we present doubly and triply differential cross sections in the vicinity of the $(2p^2)$ ^1D and $(2s2p)$ $^1P^o$ autoionizing states of helium at an incident electron energy of 250 eV. For a fixed scattering angle of 13°, abbreviated as 250 eV|13°, the measured coincidence ejected-electron spectra are compared against the measurement of Lower and Weigold [36] at 200 eV|13° and McDonald and Crowe [38] at 200 eV|12°. Note that we are working in a regime that we can neglect exchange between the scattered and the ejected electrons. Comparisons with the theoretical calculations of Godunov *et al.* [59] and Marchalant *et al.* [55] at 200 eV|12° are also made with the Shore-Balashov parameters related to the cross section for the process and the shape of the spectral line. In addition to the TDCS data, we have also taken the noncoincidence ejected-electron energy spectra.

In Sec. II we give a detailed description of the experimental apparatus and the method of analysis. Results of the $(e,2e)$ spectral measurements in the coplanar geometry are given in Sec. III, and Sec. IV presents our conclusions.

II. EXPERIMENT

A. $(e,2e)$ spectrometer

The $(e,2e)$ apparatus developed at Afyon Kocatepe University in Turkey is an electron-impact spectrometer, specially designed for electron-electron coincidence experiments. A brief description of the apparatus is reported elsewhere [43,62]. It consists of a vacuum chamber, which contains an electron gun, a Faraday cup, two identical hemispherical deflector analyzers (HDAs), and an effusive gaseous beam. The relative position of all components of the spectrometer inside the vacuum chamber is shown in Fig. 1 (top). The incident electron beam is generated by a homemade electron gun [63], capable of producing a steady beam of electrons in the energy range of 80–500 eV. The multielement electrostatic lenses were used for the geometric shaping of the electron beam. The beam diameter and the energy spread are ∼2 mm and 500 meV, respectively, as measured via the elastically scattered electrons. Beam currents ranging from a few nA to a few μA could be generated and were continuously monitored using a Faraday cup. The beam profile of the incident electrons was investigated by measuring the incident beam current as a function of the Faraday cup angle around the collision center, as shown in Fig. 2. The incident current was measured at two different electrodes, splash plate (SP) and Faraday cup (FC) (see the inset of Fig. 2), using two digital picoammeters.

The scattered and ejected electrons are analyzed in energy by two HDAs with small solid angles (0.006 sr) that image the entire collision region onto the exit plane of the hemispherical analyzer. This is achieved by coupling five-element electrostatic zoom lenses before the entry plane of the hemispherical analyzer [64]. The radius of the inner and outer hemisphere are $R_1 = 87.5$ mm and $R_2 = 112.5$ mm, which gives a mean radius of the HDA of $R_0 = 100$ mm. Energy resolutions of better than 0.1% of the incident energy (limited by the spread in the incident electron beam) were achieved. The scattered- and ejected-electron analyzers are mounted on rotary turntables, coplanar with the incident beam, which can be rotated between ±20° and 30°–135°, respectively, with reference to the incident-beam direction (where the negative angle denotes that the scattered-electron analyzer is on the opposite side of the electron beam to the ejected-electron analyzer). The effective angular range is limited by the presence of the Faraday cup in the forward angles and the electron gun in the backward angles.

Channel electron multipliers (CEMs) are used to detect the scattered and ejected electrons. In $(e,2e)$ experiments, time-correlated pulses are produced by the two CEMs when the electrons arriving at the detectors arise from the same ionizing event. This is accomplished by the coincidence electronics system illustrated in Fig. 1 (bottom). These pulses are capacitively decoupled and amplified. The amplified pulses are used to trigger the constant fraction discriminators to produce standard fast timing pulses. These fast timing pulses are then used to start and stop a time-to-amplitude converter (TAC), which measures the time difference between the pulses appearing at its start and stop inputs. The pulse originating from the scattered-electron analyzer is used as the start and the pulse originating from the ejected-electron detector is passed through a time delay unit and used as the stop. The TAC output is recorded on a pulse height analyzer (PHA), from which the true coincidence signal is determined. The TAC produces a time spectrum or histogram (counts versus time difference), which is displayed via the Trump-PCI interface card and its associated software (Maestro, ORTEC). Figure 3 shows an example of coincidence peak and a binding energy spectrum

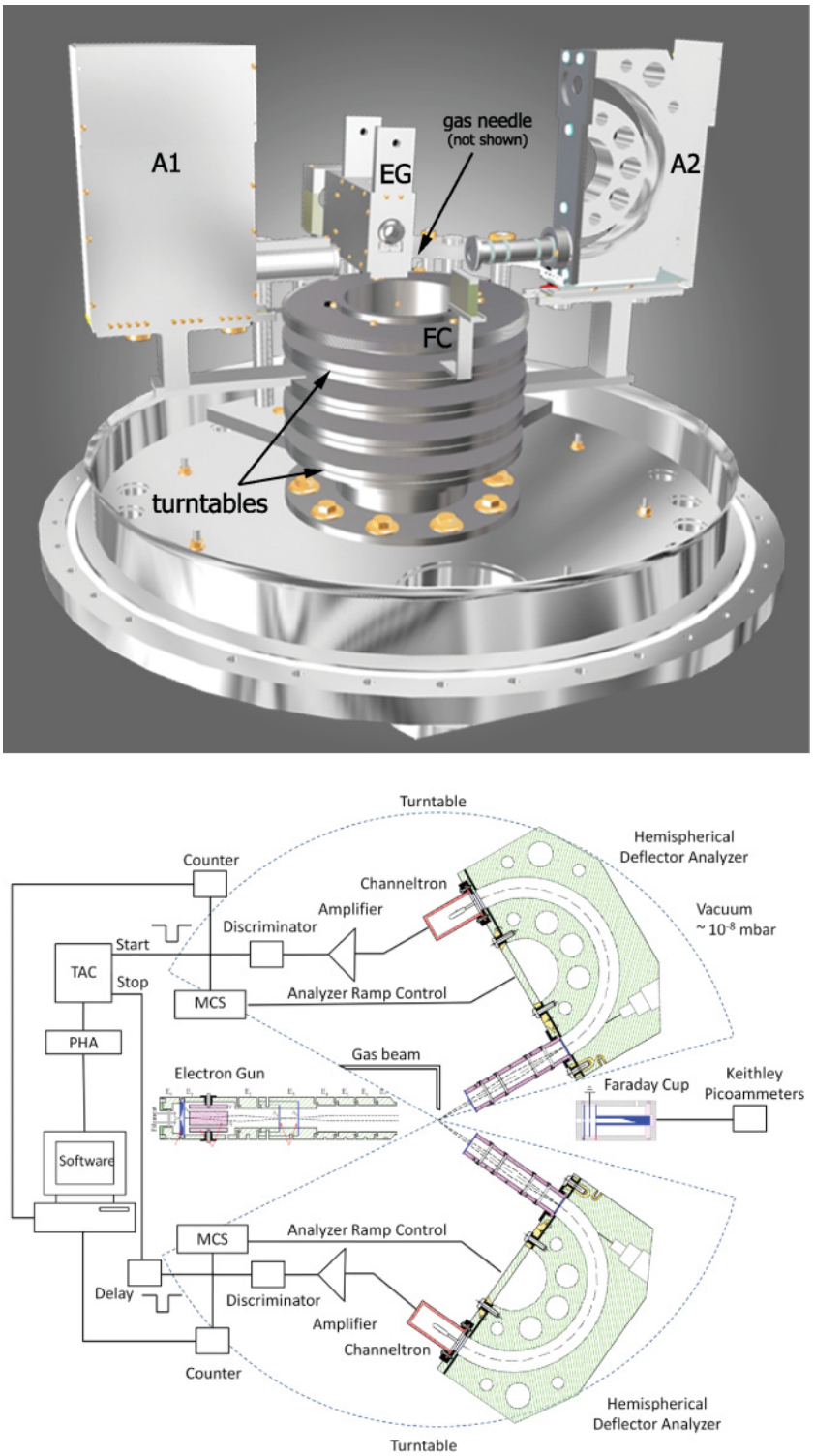

FIG. 1. (Color online) (Top) 3D drawing of the $(e,2e)$ spectrometer, showing the main sections: an electron gun (EG), two electron-energy analyzers (A1 and A2), and a Faraday cup (FC). (Bottom) A schematic diagram of the spectrometer and the electron pulse handling electronics. Electron coincidences are recorded by a time-to-amplitude converter (TAC), followed by pulse height analysis (PHA) using the electron signal from one analyzer (scattered electron) as a start pulse and the other (ejected electron) as a stop. MCS (multichannel scaling) registers the number of counts in subsequent time intervals.

of helium, a plot of the intensity of the coincidence signal obtained from TAC outputs as a function of the energy loss, in the region of the He^+ ground state at 24.59 eV. Experiments were conducted at 250-eV incident electron energy. Under these conditions the coincidence peak full width at half maximum was typically 6 ns [Fig. 3(a)], and the binding energy spectrum had an energy resolution of 0.8 eV [Fig. 3(b)]. Data acquisition is under computer control, with the PC being used to start and stop the scalar, ramp the deceleration voltage of the analyzers, monitor count rates, and other experimental conditions.

The entire spectrometer is kept in an ultrahigh vacuum chamber with suitable μ-metal shielding that reduces the ambient magnetic fields to less than 0.5 mG throughout the angular range of the analyzers. The chamber is pumped by a 500 l/s turbomolecular pump, which after sufficient baking

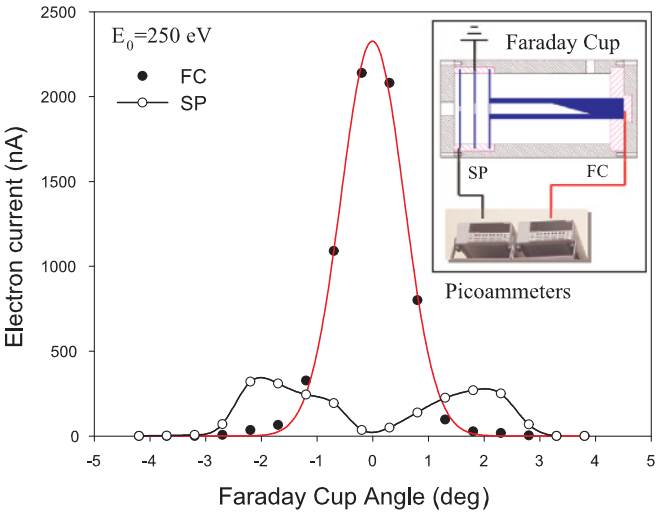

FIG. 2. (Color online) The intensity distribution of the electron current as a function of the angular displacement of the Faraday cup. The inset shows the detailed scheme of the Faraday cup electrodes. The currents measured from the FC and SP are shown by solid circles and a solid line with open circles, respectively. The Gaussian fit for the beam profile (FC) is shown with the solid (red) line.

produces a base pressure of $\sim 7 \times 10^{-8}$ mbar. The background pressure increases to $\sim 8 \times 10^{-6}$ mbar after the target gas has been introduced. All experiments are conducted under steady-state conditions which are achieved by powering all electronic equipment for sufficiently long periods of time in order to eliminate any drift in power supplies during the measurement process.

The procedure for $(e,2e)$ data acquisition involves simultaneously scanning both the ejected- and scattered-electron analyzer through the desired energy range, in opposite senses, and accumulating a coincidence timing spectrum at each energy set for a fixed ejected angular position. The energy range is scanned many times to reduce the effect of instabilities in the gun current or target pressure. Typical true coincidence count rates for these measurements range from 0.01 to 0.15 s^{-1}.

B. Method of analysis

We have analyzed the ejected-electron spectra using the Shore-Balashov parametrization [32,47,48]. In this case, the triply differential cross section can be written (for nonoverlapping resonances) in the form

$$\frac{d^3\sigma}{dE_e\, d\Omega_e d\Omega_s} = f + \sum_{\mu} \frac{A_\mu \varepsilon_\mu + B_\mu}{1+\varepsilon_\mu^2}, \qquad (1)$$

where $\varepsilon_\mu = 2(E_e - E_\mu)/\Gamma_\mu$ is the energy in half widths away from the position of the μth resonance and the sum runs over the autoionizing levels labeled by μ. For the $(2\ell 2\ell')\,^{1,3}L$ states of helium, E_μ and Γ_μ are well known, e.g., Hicks *et al.* [21]. The parameter f is simply the direct ionization cross section in the resonance region and is a slowly varying function of energy. The parameters A_μ and B_μ contain the collision dynamics and are assumed constant over the energy range of the resonance. Both parameters contain an interference term

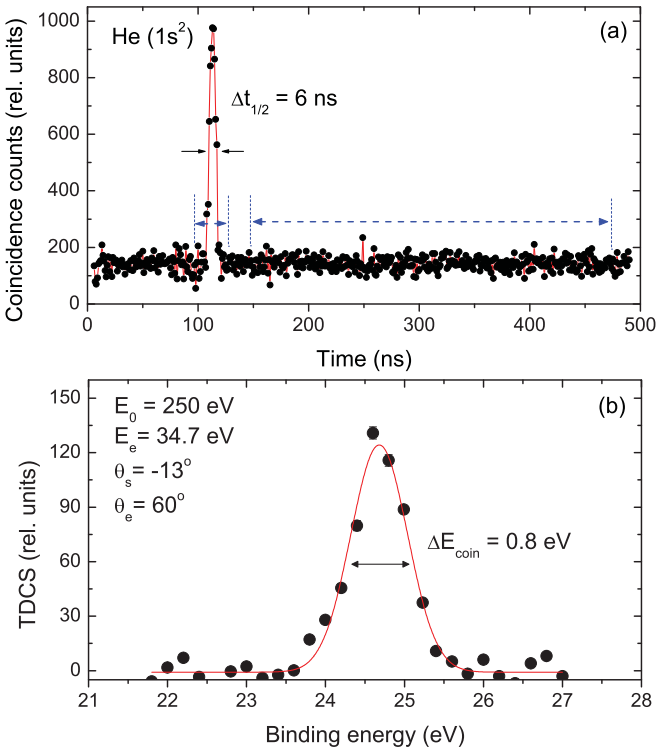

FIG. 3. (Color online) (a) Typical time delay spectrum (the points are connected by straight lines). The coincidence and background windows are also indicated. A delay (~100 ns) is employed to displace the coincidence signal from near zero time difference. (b) Binding energy spectrum of helium obtained at 250-eV impact energy. The (red) solid line shows the Gaussian fit to the spectrum.

between the direct and resonant ionization amplitudes [52], but while the A_μ parameter is composed of this term completely, the B_μ parameter has an additional term which gives the resonant cross section in the absence of any direct ionization cross section. The A_μ parameter therefore characterizes the asymmetry of the resonance profile, while the B_μ is related more to the resonance yield. From these parameters, one can extract complete information about the resonance and its interference with the continuum thus providing a sensitive test of current scattering theories.

Instead of Eq. (1) separable autoionization resonances may also be parametrized in the equivalent Fano [3] representation

$$\frac{d^3\sigma}{dE_e\, d\Omega_e d\Omega_s} = \sigma_\mu' + \sum \sigma_\mu \frac{(q_\mu + \varepsilon_\mu)^2}{1+\varepsilon_\mu^2}, \qquad (2)$$

where q_μ is the dimensionless Fano shape parameter, σ_μ is the resonance, and σ_μ' is the nonresonant direct ionization cross section. McDonald and Crowe [27] have shown that the q_μ parameter is related to the Shore-Balashov parameters A_μ and B_μ by

$$q_\mu = \frac{B_\mu \pm \left(A_\mu^2 + B_\mu^2\right)^{1/2}}{A_\mu}, \qquad (3)$$

where the sign of q_μ is the same as that of A_μ. For $(e,2e)$

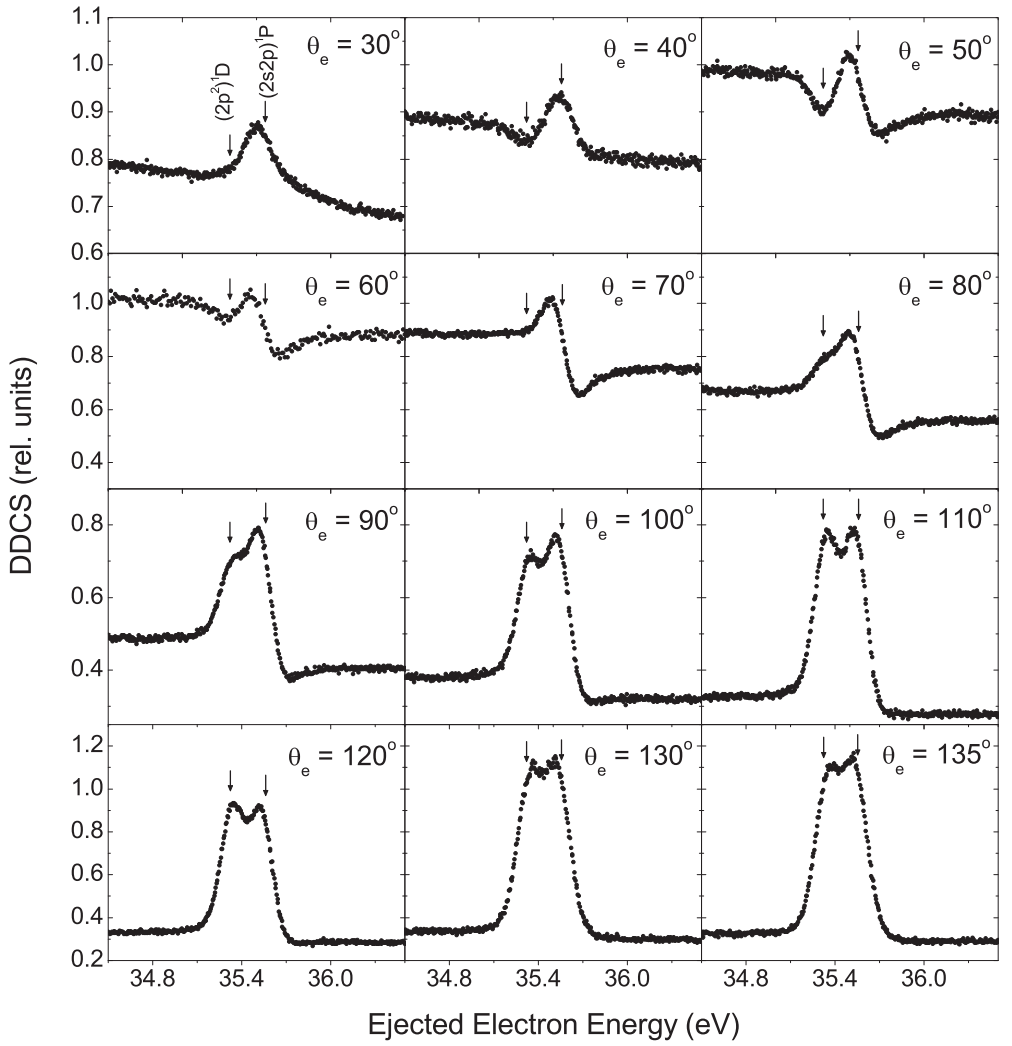

FIG. 4. Noncoincidence ejected-electron energy spectra of helium at an impact energy of 250 eV for ejection angles from 30° to 135°. The error is estimated to be ∼±3%.

processes, the Shore-Balashov parametrization in Eq. (1) is to be preferred to the Fano representation [38].

For the present spectral $(e,2e)$ measurements, the spectrometer was operated in the following way: The energy of the incident electron beam was 250 eV. One analyzer measured "ejected" electrons over a range of energies between 35 and 36 eV, a region encompassing the ^1D and $^1P^o$ resonant states. "Scattered" electrons were collected in the second analyzer over a complementary 1-eV range, the position of which was determined by energy conservation. In the present work the scattered-electron analyzer was fixed at -13°, while the coincidence ejected-electron spectra were measured over the range 30°–130° of ejection angles in the binary region. The recoil region of the cross section was measured independently by moving the scattered-electron analyzer from -13° to $+13^\circ$. At each ejection angle, the measured spectrum is fitted, in a least-squares fit analysis, with the usual Shore-Balashov function. We note that the form of the Shore-Balashov equation is convoluted with the instrumental response in the fit. We have calibrated the energy scale of our spectrum against the high-resolution measurements of Hicks *et al*. [21].

III. RESULTS AND DISCUSSION

We have studied electron ejection from the $(2p^2)\ ^1D$ and $(2s2p)\ ^1P^o$ autoionizing states of helium having ejected-electron energies of 35.32 and 35.56 eV, respectively. The ejected-electron angular distributions and energy spectra have been measured both in singles and in coincidence with the scattered electrons and compared with the available experimental and theoretical data. The Shore-Balashov parameters have been determined by the procedure outlined.

A. Noncoincidence results

Figure 4 shows the noncoincidence ejected-electron energy spectra in the vicinity of the ^1D and $^1P^o$ autoionizing states of helium at different ejection angles. The spectra are differential in energy and angle and are referred to as the relative DDCSs. The parameters f, A_μ, and B_μ extracted from these spectra are shown in Fig. 5 as a function of ejected-electron angle. The measured parameters are compared with other experimental data where available. The DDCS for direct ionization f shows a maximum ∼50°. The DDCS results of Müller-Fiedler *et al*.

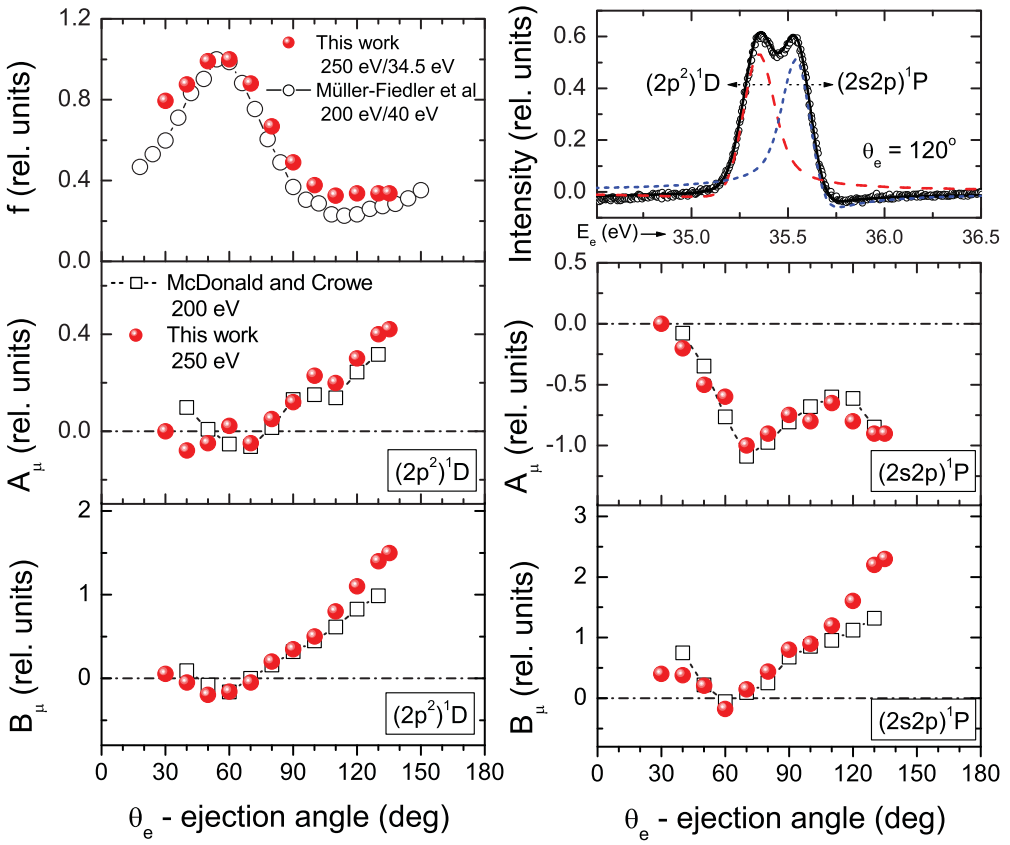

FIG. 5. (Color online) The Shore-Balashov parameters A_μ and B_μ and the direct ionization cross section f from the noncoincidence ejected-electron spectra given in Fig. 4 as a function of ejected-electron angle for the ^1D and $^1P^o$ states of helium at an incident energy of 250 eV. The top right-hand panel shows an example of the measured spectrum at 120°. The long-dashed and short-dashed lines indicate the contributions of ^1D and $^1P^o$ resonances, respectively, convoluted with our instrumental resolution (150 meV) and the solid line the overall fit to the data.

[65] at 200-eV incident energy and 40-eV ejected-electron energy have been used for comparison. The only previous experimental data with which the present Shore-Balashov parameters can be compared are those of McDonald and Crowe [26] at an incident energy of 200 eV.

The resonance contributions together with the strong background of direct ionization processes lead to a complicated asymmetric structure of the resonance profile in the DDCS. A strong overlap also occurs because of the very close proximity of these levels to each other. The spectra are nearly peaklike with little asymmetry at the backward angles and exhibit drastic changes with the ejection angle. The top right-hand panel of Fig. 5 shows a typical example of the measured spectrum, the fit to the data, and the final form of the resonance profile obtained from the convolution. The ^1D state is optically forbidden, but at backward angles is strongly enhanced. The $^1P^o$ state remains a recognizable peak shape in all the spectra, particularly in the backward direction. The $^1P^o$ state is excited by direct dipole transition and is therefore a very important resonance.

The A_μ and B_μ parameters for the ^1D state have a single dip at 60°–70° and a relatively large positive peak for backward angles. The large positive values of B_μ are a confirmation of constructive interference while the negative values indicate destructive interference. For the $^1P^o$ state, the A_μ parameter behavior is oscillatory and predominantly negative. The B_μ parameter is positive at all angles except at 60°, where it becomes slightly negative, and is of comparable magnitude to the corresponding A_μ parameter. Agreement between the data of McDonald and Crowe [26] is quite good for angles below 100°, but above the present B_μ parameters tend to have higher values.

B. Coincidence results

Figures 6 and 7 show the coincidence $(e,2e)$ spectra measured in the binary and recoil region for the ^1D and $^1P^o$ autoionizing states. The corresponding Shore-Balashov parameters A_μ and B_μ deduced from the fitting of the individual spectra are shown in Fig. 8. The experimental results are presented together with the results of Lower and Weigold [36] and McDonald and Crowe [38], which are the only experimental data available for comparison. In Fig. 8, the Shore-Balashov parameters are also compared to the theoretical TDCS calculations of Godunov *et al.* [59] and Marchalant *et al.* [55]. Since their original spectral data are not available, we have used their published Shore-Balashov parameters to obtain the profiles. Their resonance profiles are convoluted with our experimental resolution of 150 meV. For each experiment and theory the parameters A_μ, B_μ, and f

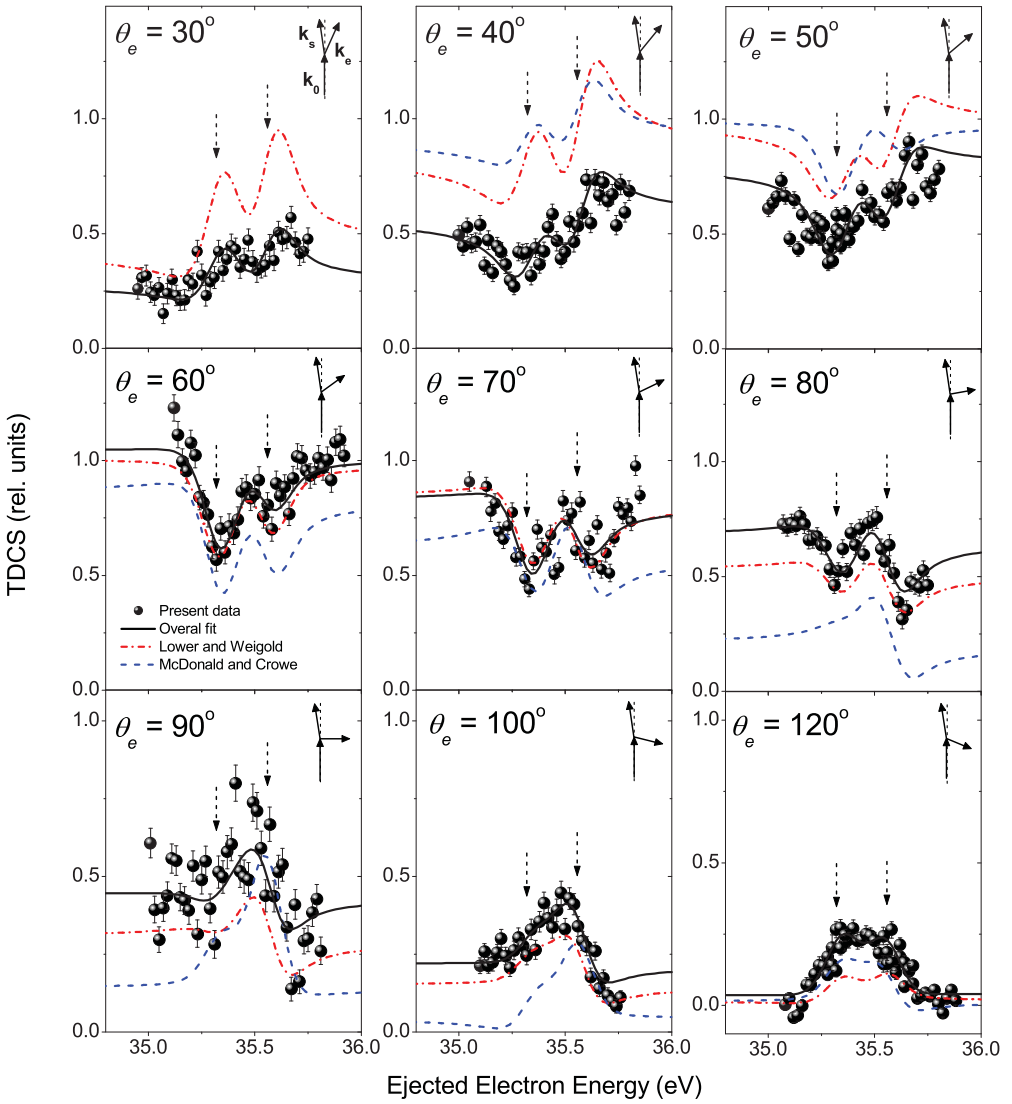

FIG. 6. (Color online) Coincidence $(e,2e)$ ejected-electron energy spectra in the vicinity of the $(2p^2)\,{}^1D$ and $(2s2p)\,{}^1P^o$ states of helium in the binary region for an incident energy of 250 eV and a scattering angle of -13°, corresponding to a momentum transfer of 1.06 a.u. Solid circles: Present experimental data. Solid line: A fit of the Shore-Balashov parametrization to the data. The vertical bars represent the statistical errors. Dashed-dotted line: Lower and Weigold [36]. Dashed line: McDonald and Crowe [38]. The downward pointing arrows indicate the positions of the ${}^1D$ and ${}^1P^o$ resonances. The incident k_0, detected ejected k_e, and scattered k_s electron directions are also indicated.

have the same relative scale and the direct ionization cross section f at the $(2s^2)\,{}^1S$ resonance was normalized to unity at one angle ($\theta_e = 60^\circ$ for the present experiment and $\theta_e = 50^\circ$ for the previous experiments and calculations), as the two parameters are then automatically normalized. Therefore, the values of the resonant parameters are consistent between the experiments and theories.

In the binary peak region, asymmetric profiles are evident in the $(e,2e)$ spectra (see Fig. 6), but in the recoil peak direction the ${}^1D$ and ${}^1P^o$ states appear enhanced and peaklike (see Fig. 7), though this does not of course preclude interference effects. Note that the ${}^1P^o$ resonance yield is small as compared with the maxima of the ${}^1D$ resonance yield in the recoil region. With increasing ejection angle from -130° to -50° the yield of the optically allowed ${}^1P^o$ resonance grows relative to the yield of ${}^1D$ resonance. The results of McDonald and Crowe [38] lie above the experimental data points in the recoil region. This is expected due to the different values of the incoming electron energy. The results of Lower and Weigold [36] lie somewhat below the experimental data points in the recoil peak direction, even for direct ionization. We also observe distinctly different profiles than those of Lower and Weigold [36] at -50° and -60°.

In Fig. 8, the A_μ and B_μ parameters for both resonances show a rapid variation with ejected-electron angle indicating their sensitivity to the interference process. In this case their oscillatory character could be attributed to the angular momentum or symmetry of the state. In the binary peak region, the A_μ and B_μ parameters of the ${}^1D$ state show a sharp negative minimum $\sim 60^\circ$, followed by a broad positive maximum. In the recoil region both parameters increase positively with increasing ejection angle. For the ${}^1P^o$ state, the A_μ parameter is predominantly negative in both regions. The B_μ parameter dips sharply negative at 60° and then positive to peak again

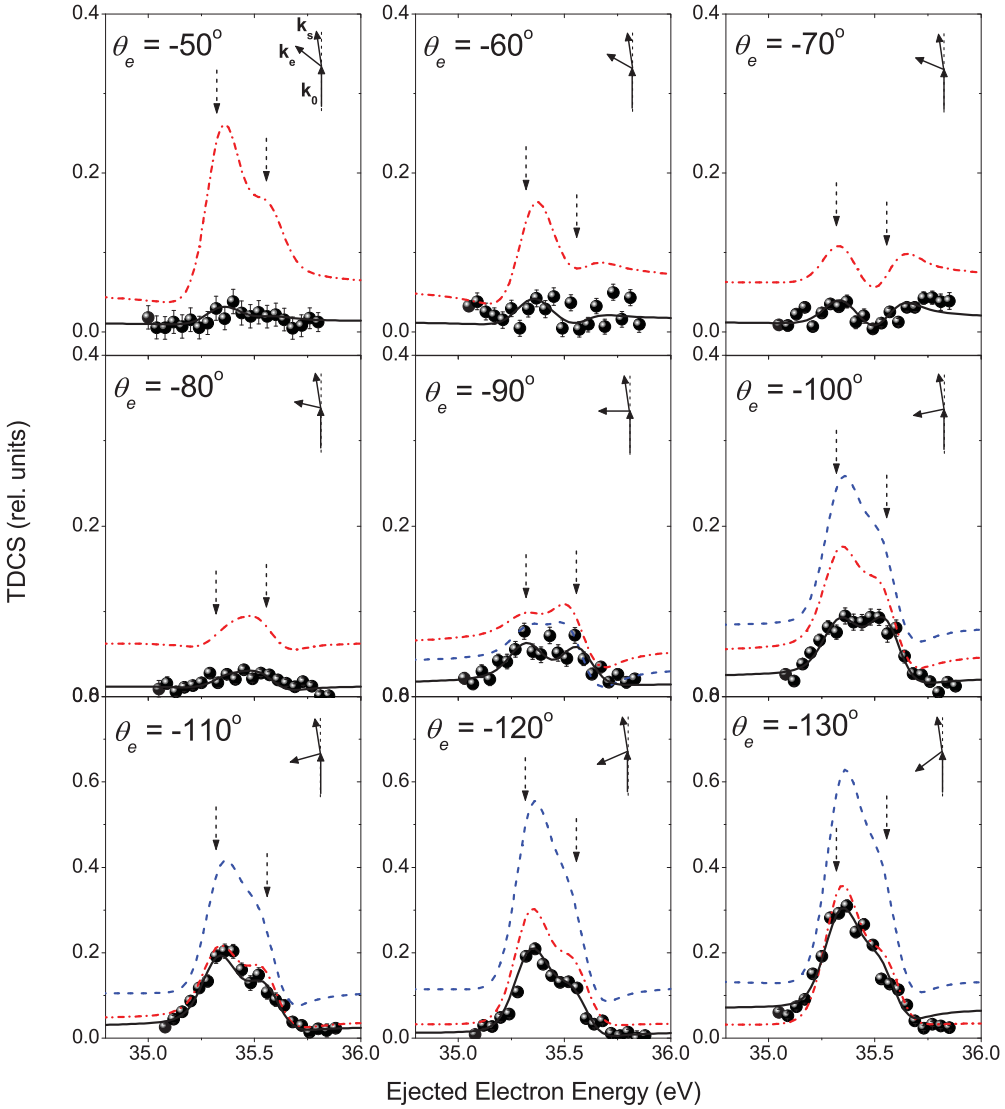

FIG. 7. (Color online) Same as Fig. 6, but for the recoil region.

at 100°, while in the recoil region it increases positively with increasing ejection angle. Note that the spectra and resonant parameters given in these figures are quite different in shape and magnitude to the corresponding noncoincidence results given in Figs. 4 and 5. In general, there is qualitatively good agreement between the present and the previous experimental data for the resonant parameters. Where differences do occur, they are found mainly at backward angles (above −100°) and forward angles (below 60°). In Fig. 8, Lower and Weigold [36] observed a dip in the value of the resonant parameters at∼−80°, which is not seen in the present experimental data.

Unlike the earlier studies, the present study was undertaken at an incident electron energy of 250 eV, while the previous works were done at an incident energy of 200 eV. Therefore, the relative contribution of interfering resonant and direct ionization is expected to change. The main differences will be in the shift of the binary peak for the direct ionization away from the momentum transfer direction as well as in the magnitude of the recoil peak.

Figure 9(a) is the angular distribution for direct ionization, where we present the TDCS results for an ejected-electron energy of 34.5 eV. The present data displays a maximum at ∼60°, definitely displaced with respect to the momentum transfer direction, which in the present experiment is approximately $\theta_K = 53°$. Note that the values of θ_K are 45° for Ref. [36] and 44° for Ref. [38]. An ∼10° shift can be seen in the position of the present binary peak relative to the early experiments, consistent with the change in momentum directions. The same TDCS results, but, at the resonance energies of the ^1D and $^1P^o$ states are also shown in Figs. 9(b) and 9(c). For the resonance states, the previous experimental results deviate strongly from the present data in the angular range between 30° and 60°, with their results showing a local maximum near 40° and a decreasing cross section below 40°. By contrast, the present experimental data decreases rapidly below 60°. This discrepancy is presumably the result of using different incoming electron energies.

For direct ionization the binary peak is the dominant one for our kinematical situation and the recoil peak essentially

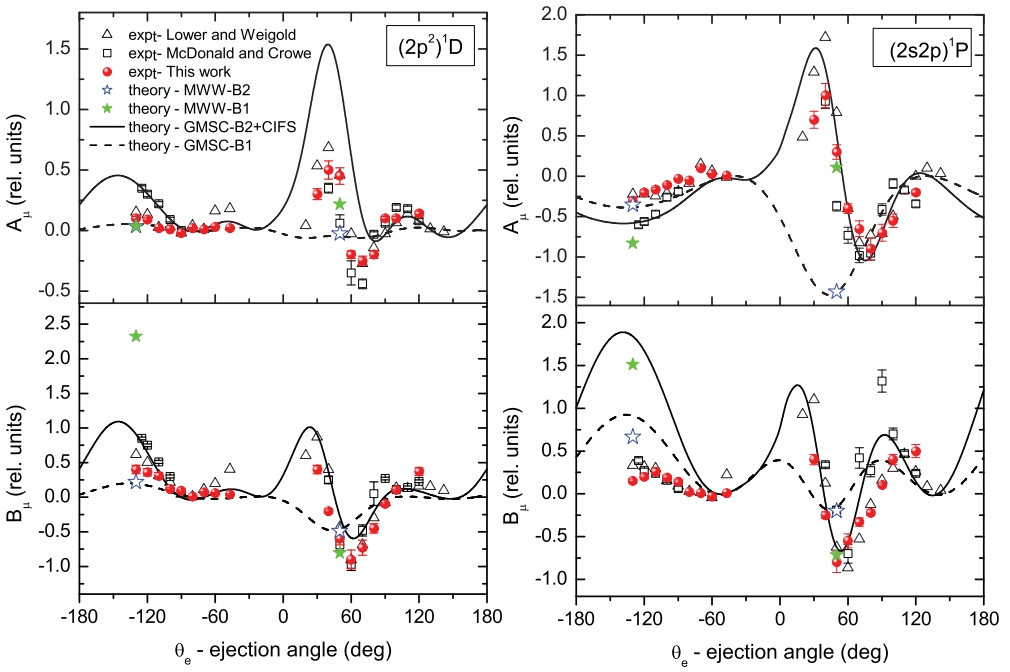

FIG. 8. (Color online) The Shore-Balashov resonant parameters A_μ and B_μ for the ^1D and $^1P^o$ states as a function of the ejection angle. Experimental results: Solid circles, present results at 250 eV|13°; open triangles, results of Lower and Weigold [36] at 200 eV|13°; open squares, results of McDonald and Crowe [38] at 200 eV|12°. Theoretical results of Godunov *et al.* [59]: Solid line, second Born calculations with CIFS (GMSC-B2 + CIFS); dashed line, calculations in the first Born approximation (GMSC-B1). Theoretical results of Marchalant *et al.* [55]: Solid stars, second Born calculations (MWW-B2); open stars, first Born calculations (MWW-B1).

vanishes. In Figs. 8 and 9, a smaller recoil peak is observed in present experimental data for both the resonant parameters and TDCS results than in previous experiments. This is due to the different values of incoming electron energy. Furthermore, the presence of autoionization results in a clearly visible recoil peak in Figs. 9(b) and 9(c) with a shape that was strongly dependent on the orbital angular momentum L of the resonance. A noncoplanar $(e,2e)$ investigation was recently published on helium with the same conclusions [61]. Although the system and kinematics investigated here are very different from those in the study of Ref. [61], some experimental insight may be gained from a qualitative comparison between coplanar and noncoplanar experiments for autoionization of helium.

In Figs. 8 and 9, the parameters and TDCS results are compared with the calculation of Godunov *et al.* [59]. It is clear that second-order approximations with inclusion of the three-body Coulomb interaction in the final state (CIFS) have greatly improved the situation over the first Born approximation. However, looking at the recoil region for the $^1P^o$ resonance yield parameter B_μ we see that the first and second Born results are approximately two and four times larger than the experimental values, respectively. Note that the parameter B_μ gives the height of the resonance. Indeed, the first Born value for the height of the $^1P^o$ cross section is always much closer to experiment than the second Born prediction. We note that, in the same kinematical case, the second Born theory of Marchalant *et al.* [55] predicts a larger value of the B_μ parameter for the ^1D state at the recoil region than the theory of Godunov *et al.* [59]. We see a factor-of-3 difference. In this case, however, it is currently unclear why such a strong discrepancy is observed. This anomaly should be investigated further. The second Born calculation shown in Fig. 9 is in fair agreement with experiments except for the smaller ejected-electron angles where the binary peak in the present experiment is displaced further away from the direction of the momentum transfer (shown as an arrow in the figure). The manifest difference, which becomes obvious when comparing theory and experiment, is increasing relative recoil peak intensity in Fig. 9(b) for the $^1P^o$ resonance, which, conversely, decreases in all experiments.

Figure 10 compares the $(e,2e)$ ejected-electron spectra of the first and second Born calculations of Godunov *et al.* [59] and Marchalant *et al.* [55] with the present and previous experimental data in the binary and recoil peak direction, 50° and −130°. The agreement between the second-order theory and experiment is particulary good. At −130°, the second Born calculation of Godunov *et al.* [59] gives ^1D and $^1P^o$ resonances of comparable height, while the present and previous experiments indicate that the ^1D resonance is higher than the $^1P^o$ resonance. However, the shape of the experimental data and second Born cross sections of Marchalant *et al.* [55] shows good agreement, although the second-order results for the A_μ and B_μ parameters are much larger than experiment. Nevertheless, the second Born approximation of Marchalant *et al.* [55] predicts that the ^1D peak will be slightly larger than the $^1P^o$ peak, while the first Born approximation predicts that the ^1D contribution will only be a small shoulder on the low-energy side of a pronounced $^1P^o$ peak.

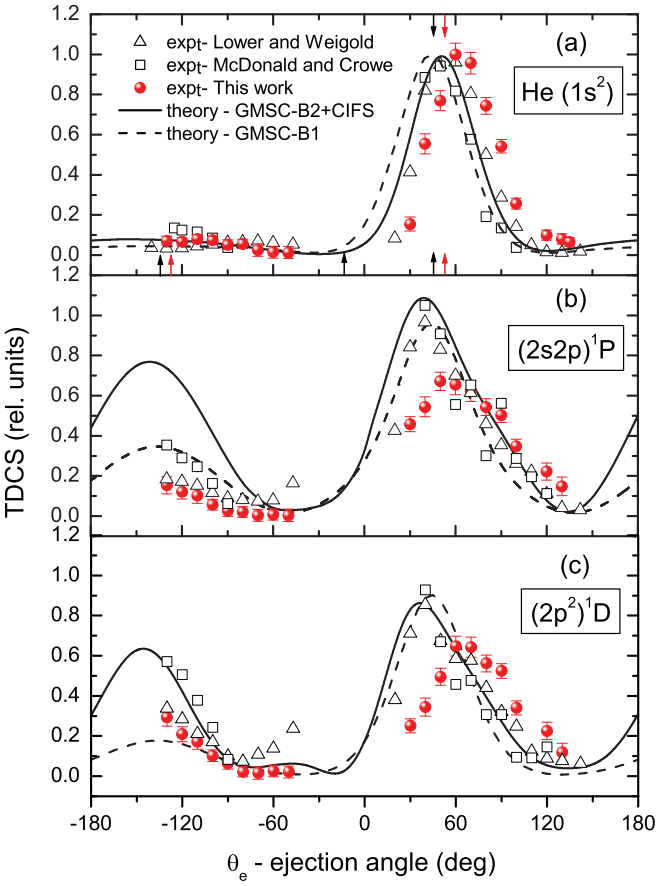

FIG. 9. (Color online) Helium $(e,2e)$ ejected-electron angular distributions for 250 eV electrons scattered through $-13^\circ$and for (a) direct ionization, (b) $(2s2p)\,^1P^o$, and (c) $(2p^2)\,^1D$ states. The vertical bars represent the experimental results and include statistical errors. Full circles denote our experimental results, while the triangles and squares are those of Lower and Weigold [36] and McDonald and Crowe [38]. The arrows indicate the momentum transfer direction. The direct ionization cross section has been obtained at an ejected-electron energy of 34.5 eV. Theoretical results of Godunov *et al.* [59]: Solid line, second Born calculations with CIFS (GMSC-B2 + CIFS); dashed line, first-order Born approximation calculations (GMSC-B1).

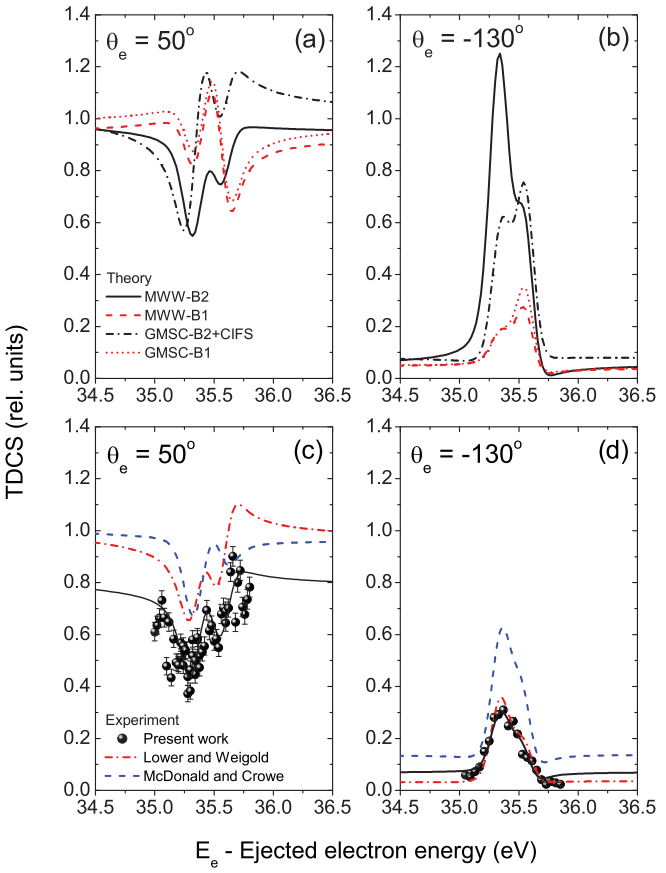

FIG. 10. (Color online) $(e,2e)$ ejected-electron spectra for 250-eV incident energy and -13° scattering angle in the binary and recoil peak direction, 50° and -130°. The upper panel shows the first and second Born calculations and the lower panel the experimental measurements.

IV. SUMMARY AND CONCLUSION

In this paper we have presented recent measurements of the doubly and triply differential cross sections for autoionizing states of helium in the energy region of the $(2p^2)\,^1D$ and $(2s2p)\,^1P^o$ resonances using a newly developed $(e,2e)$ spectrometer. Asymmetric coplanar kinematics have been used to study the autoionizing $(e,2e)$ spectra. These results have shown the contrasting roles of the nondipole transition of the $(2p^2)\,^1D$ and the $(2s2p)\,^1P^o$ dipole one. For most cases, the resonance profiles and parameters agree well with previous experimental results. However, some differences were found at forward and backward directions compared with previous experimental studies. These differences in the shape and magnitude of the cross sections are attributed to the different incoming electron energies used in the experiments.

Comparing the TDCS results at the resonance energies where ionization can be formed either directly or indirectly via an autoionizing state provides us with the opportunity to study the interference effects between the direct ionization and autoionization process. For the kinematical condition investigated, the yields of the ^1D resonance dominates over the $^1P^o$ resonance yield for ejection angles between $-100^\circ$and -130° in the recoil peak region, where autoionization dominates direct ionization, and the resonances are clearly visible above the direct ionization background. Therefore, the characteristics of the TDCS are sensitive to the orbital angular momentum L of the resonance. Our conclusions support similar findings by deHarak *et al.* [61] at higher energies. Since a sensitive test of theory is the ability to obtain the correct binary-recoil intensity ratio, the relationship between the TDCS for different autoionizing states is an important consideration, from the standpoints of theory [66].

The second-order theory of Godunov *et al.* [59] was found to be in good agreement with the general shape of the resonant parameters. The Coulomb interaction in the final state (CIFS) between the scattered electron, ejected electron, and residual ion can strongly influence both direct ionization and resonance parameters (f,A_μ,B_μ) around the binary lobe. However, the $^1P^o$ resonance yield parameter B_μ is significantly overestimated at the recoil region by a factor of 2–4, which results in a relatively large recoil peak in blunt contradiction to the experiment. This indicates that the

theoretical description of the excitation with autoionization mechanism has yet to be solved. We hope that our results will stimulate the further development of theoretical approaches in this field.

A further study of the angular distributions of ejected electrons from autoionizing states at lower energies and different scattering angles is in progress. In this way, the momentum transfer dependence of the resonance profiles will be explored.

ACKNOWLEDGMENTS

We are thankful to A. L. Godunov for providing us the calculated data of the resonant parameters for the ^1D and $^1P^o$ autoionizing states of helium, along with their recent publications. The authors would like to express thanks to Theo J. M. Zouros for carefully reading the manuscript. This work was partially supported by the Scientific and Technological Research Council of Turkey (TUBITAK) through Grants No. 106T722 and No. 109T738.

[1] G. Tanner, K. Richter, and J. M. Rost, Rev. Mod. Phys. **72**, 497 (2000).
[2] R. P. Madden and K. Codling, Astrophys. J. **141**, 364 (1965).
[3] U. Fano, Phys. Rev. **124**, 1866 (1961).
[4] U. Fano and J. W. Cooper, Phys. Rev. **137**, A1364 (1965).
[5] U. Fano and J. W. Cooper, Rev. Mod. Phys. **40**, 441 (1968).
[6] M. Domke, C. Xue, A. Puschmann, T. Mandel, E. Hudson, D. A. Shirley, G. Kaindl, C. H. Greene, H. R. Sadeghpour, and H. Petersen, Phys. Rev. Lett. **66**, 1306 (1991).
[7] M. Domke, G. Remmers, and G. Kaindl, Phys. Rev. Lett. **69**, 1171 (1992).
[8] M. Domke, K. Schulz, G. Remmers, A. Gutierrez, G. Kaindl, and D. Wintgen, Phys. Rev. A **51**, R4309 (1995).
[9] K. Schulz, G. Kaindl, M. Domke, J. D. Bozek, P. A. Heimann, A. S. Schlachter, and J. M. Rost, Phys. Rev. Lett. **77**, 3086 (1996).
[10] M. Domke, K. Schulz, G. Remmers, G. Kaindl, and D. Wintgen, Phys. Rev. A **53**, 1424 (1996).
[11] M. Inokuti, Rev. Mod. Phys. **43**, 297 (1971).
[12] T. J. M. Zouros, D. Schneider, and N. Stolterfoht, Phys. Rev. A **35**, 1963 (1987).
[13] D. R. DeWitt, R. Schuch, T. Quinteros, H. Gao, W. Zong, H. Danared, M. Pajek, and N. R. Badnell, Phys. Rev. A **50**, 1257 (1994).
[14] S. M. Silverman and E. N. Lassettre, J. Chem. Phys. **40**, 1265 (1964).
[15] J. A. Simpson, G. E. Chamberlain, and S. R. Mielczarek, Phys. Rev. **139**, A1039 (1965).
[16] H. F. Wellenstein, R. A. Bonham, and R. C. Ulsh, Phys. Rev. A **8**, 304 (1973).
[17] X. W. Fan and K. T. Leung, J. Phys. B **34**, 811 (2001).
[18] X. J. Liu, L. F. Zhu, Z. S. Yuan, W. B. Li, H. D. Cheng, Y. P. Huang, Z. P. Zhong, K. Z. Xu, and J. M. Li, Phys. Rev. Lett. **91**, 193203 (2003).
[19] S. J. Brotton, S. Cvejanovic, F. J. Currell, N. J. Bowring, and F. H. Read, Phys. Rev. A **55**, 318 (1997).
[20] G. Gelebart, R. J. Tweed, and J. Peresse, J. Phys. B **7**, L174 (1974).
[21] P. J. Hicks, S. Cvejanović, J. Comer, F. H. Read, and J. M. Sharp, Vacuum **24**, 573 (1974).
[22] P. J. Hicks and J. Comer, J. Phys. B **8**, 1866 (1975).
[23] G. Gelebart, R. J. Tweed, and J. Peresse, J. Phys. B **9**, 1739 (1976).
[24] N. Oda, S. Tahira, F. Nishimura, and F. Koike, Phys. Rev. A **15**, 574 (1977).
[25] J. P. van den Brink, G. Nienhuis, J. van Eck, and H. G. Heideman, J. Phys. B **22**, 3501 (1989).
[26] D. G. McDonald and A. Crowe, J. Phys. B **25**, 2129 (1992).
[27] D. G. McDonald and A. Crowe, J. Phys. B **25**, 4313 (1992).
[28] B. A. deHarak, J. G. Childers, and N. L. S. Martin, Phys. Rev. A **74**, 032714 (2006).
[29] H. Ehrhardt, K. Jung, G. Knoth, and P. Schlemmer, Z. Phys. D **1**, 3 (1986).
[30] A. Lahmam-Bennani, J. Phys. B **24**, 2401 (1991).
[31] E. Weigold and I. E. McCarthy, *Electron Momentum Spectroscopy* (Plenum, New York, 1999).
[32] V. V. Balashov, S. S. Lipovetskii, and V. S. Senashenko, Sov. Phys. JETP **36**, 858 (1973).
[33] E. Weigold, A. Ubgabe, and P. J. O. Teubner, Phys. Rev. Lett. **35**, 209 (1975).
[34] A. Pochat, R. J. Tweed, M. Dorich, and J. Peresse, J. Phys. B **15**, 2269 (1982).
[35] P. S. K. Moorhead and A. Crowe, in *Proceedings of the 14th International Conference on the Physics of Electronic and Atomic Collisions (Palo Alto)*, edited by D. L. H. M. J. Coggiola and R. P. Saxon (North-Holland, Amsterdam, 1985), p. 160.
[36] J. Lower and E. Weigold, J. Phys. B **23**, 2819 (1990).
[37] D. G. McDonald and A. Crowe, Z. Phys. D **23**, 371 (1992).
[38] D. G. McDonald and A. Crowe, J. Phys. B **26**, 2887 (1993).
[39] O. Samardzic, A. S. Kheifets, E. Weigold, B. Shang, and M. J. Brunger, J. Phys. B **28**, 725 (1995).
[40] M. J. Brunger, O. Samardzic, A. S. Kheifets, and E. Weigold, J. Phys. B **30**, 3267 (1997).
[41] O. Samardzic, L. Campbell, M. J. Brunger, A. S. Kheifets, and E. Weigold, J. Phys. B **30**, 4383 (1997).
[42] B. A. deHarak, J. G. Childers, and N. L. S. Martin, J. Electron. Spectrosc. Relat. Phenom. **141**, 75 (2004).
[43] O. Sise, M. Dogan, I. Okur, and A. Crowe, J. Phys. B **43**, 185201 (2010).
[44] O. Sise, M. Dogan, I. Okur, and A. Crowe (unpublished).
[45] A. Crowe and M. Dogan, *Electron Scattering from Atoms, Molecules, Nuclei and Bulk Matter* (Kluwer Academic/Plenum, New York, 2005), pp. 13–22.
[46] O. Lhagva, R. Badamdamdin, S. I. Strakhova, and L. Hehnmedeh, Z. Phys. D **27**, 259 (1993).
[47] B. W. Shore, Rev. Mod. Phys. **39**, 439 (1967).
[48] R. J. Tweed, J. Phys. B **9**, 1725 (1976).
[49] A. Crowe, D. G. McDonald, S. E. Martin, and V. V. Balashov, Can. J. Phys. **74**, 736 (1996).
[50] V. V. Balashov, S. E. Martin, and A. Crowe, J. Phys. B **29**, L337 (1996).
[51] K. Balt-Erdene, L. Henmedekh, O. Lhagva, and J. N. Madsen, J. Phys. B **32**, L35 (1999).

[52] R. J. Tweed and J. Langlois, J. Phys. B **19**, 3583 (1986).
[53] A. S. Kheifets, J. Phys. B **26**, 2053 (1993).
[54] I. E. McCarthy and B. Shang, Phys. Rev. A **47**, 4807 (1993).
[55] P. J. Marchalant, C. T. Whelan, and H. R. J. Walters, *Coincidence Studies of Electron and Photon Impact Ionization* (Plenum, New York, 1997), pp. 21–43.
[56] Y. Fang and K. Bartschat, J. Phys. B **34**, L19 (2001).
[57] Y. Fang and K. Bartschat, J. Phys. B **34**, 2747 (2001).
[58] P. J. Marchalant, Ph.D. thesis, The Queen's University of Belfast, 1996.
[59] A. L. Godunov, J. H. McGuire, V. A. Schipakov, and A. Crowe, J. Phys. B **35**, L245 (2002).
[60] B. A. deHarak, K. Bartschat, and N. L. S. Martin, Phys. Rev. Lett. **100**, 063201 (2008).
[61] B. A. deHarak, K. Bartschat, and N. L. S. Martin, Phys. Rev. A **82**, 062705 (2010).
[62] M. Dogan, M. Ulu, and O. Sise, J. Electron. Spectrosc. Relat. Phenom. **161**, 58 (2007).
[63] M. Ulu, O. Sise, and M. Dogan, Radiat. Phys. Chem. **76**, 636 (2007).
[64] M. Dogan, O. Sise, and M. Ulu, Radiat. Phys. Chem. **76**, 445 (2007).
[65] R. Muller-Fiedler, K. Jung, and H. Ehrhardt, J. Phys. B **19**, 1211 (1986).
[66] A. S. Kheifets, A. Naja, E. M. S. Casagrande, and A. Lahmam-Bennani, J. Phys. B **42**, 165204 (2009).